Random-lattice models and simulation algorithms for the phase equilibria in two-dimensional condensed systems of particles with coupled internal and translational degrees of freedom

Morten Nielsen,[1] Ling Miao,[1] John H. Ipsen,[2] Ole G. Mouritsen,[2] and Martin J. Zuckermann[1]

[1]*Centre for the Physics of Materials, Department of Physics, McGill University, Montréal, Québec, Canada H3A 2T8*

[2]*Department of Chemistry, Building 206, The Technical University of Denmark, DK-2800 Lyngby, Denmark*

(Received 7 May 1996)

In this work we concentrate on phase equilibria in two-dimensional condensed systems of particles where both translational and internal degrees of freedom are present and coupled through microscopic interactions, with a focus on the manner of the *macroscopic* coupling between the two types of degrees of freedom. First, an unconventional description of the translational degrees of freedom is developed, in which the randomly varying spatial connectivity of the particles is represented by a *random lattice* whose dynamic structure is given by triangulating the spatial configurations. Based on this random-lattice description, a series of three statistical-mechanical models are then constructed. All of the three models are in essence spin-1/2 Ising models where the spins, representing internal degrees of freedom, are associated with hard-disk particles and nearest-neighbor particles interact through spin-spin interactions that may have spatial dependence. The *fluctuating* number of nearest neighbors and the possible spatial dependence of the spin-spin interactions couple microscopically the spin degrees of freedom to the translational degrees of freedom. The first model (I) is a random-lattice Ising model with conventional nearest-neighbor spin-spin interactions. The second model (II) is an extension of this model to include a spatial dependence of the nearest-neighbor spin-spin interactions. The third model (III) is a modification of the second model that accounts for spin states with different internal degeneracy. Monte Carlo simulation techniques, including both a special algorithm for the random-lattice description and histogram and finite-size scaling analysis, are used to investigate the phase behavior of all three models. It is shown that the order-disorder spin transition in model I is decoupled from a first-order singularity—lattice melting—associated with the translational degrees of freedom and remains critical and falls in the universality class of the standard two-dimensional Ising model on regular lattices. Model II is shown to exhibit a phase diagram that has a region where the spin degrees of freedom are slaved by the translational degrees of freedom and develop a first-order singularity in the order-disorder transition that accompanies the lattice-melting transition. The internal degeneracy of the spin states in model III implies that the spin order-disorder singularity can be of first order throughout the phase diagram. It is found that this first-order singularity can be either coupled to or decoupled from the lattice-melting singularity, depending on the strength of the microscopic coupling. The calculated phase diagram and the associated thermodynamic transitional properties for model III are discussed in relation to experiments on planar bilayers of lipid-chain molecules whose properties are determined by a subtle coupling between the translational variables and the intrachain conformational states. [S1063-651X(96)01212-3]

PACS number(s): 02.70.−c, 64.60.Cn, 05.50.+q

I. INTRODUCTION

Ordering phenomena involving both translational and internal molecular degrees of freedoms are common in amphiphilic and liquid-crystal systems [1]. One specific class of systems involves hydrated bilayers composed of lipids that are amphiphilic molecules [2]. Each monolayer in a lipid bilayer constitutes a two-dimensional (2D) condensed system of interacting lipid molecules with internal degrees of freedom corresponding to chain conformational states. It is well established that a lipid-bilayer system exhibits various thermodynamic transitions [3], among which the most prominent and most studied one is the main phase transition. It is usually assumed that this thermotropic transition involves two distinct but coupled phase transitions—2D lattice melting and chain melting—associated with the translational and chain conformational degrees of freedom, respectively [3]. In other words, the transition takes the bilayer from a low-temperature (gel) phase, which is a solid and has (quasi) long-range translational order and a high degree of confor-

mational order within the lipid chains, to a high-temperature (fluid or liquid-crystalline) phase, which displays disorder in both the translational and chain conformational degrees of freedom.

In a first approximation the main transition in lipid bilayers can be described in terms of simple lattice models, where each lattice site is assigned a lipid chain with an internal variable—analogous to an Ising spin variable in the standard regular-lattice Ising model—representing the conformational degree of freedom [4] and where neighboring chains interact in a way that depends on the values of their internal variables, analogous to Ising-like spin-exchange interactions. This approach has been quite successful in describing several essential thermodynamic properties of the main transition that are mainly related to the chain conformational degrees of freedom [5]. However, it does not take into consideration the interplay between the conformational (or internal) and translational degrees of freedom, an important issue in understanding the structural properties and thermodynamic behavior of the systems. For example, both the surface density

of the bilayer and the lateral mobility of individual lipid molecules strongly depend on the chain conformational states. In several cases, experiments have clearly revealed manifestations of this interplay. A prominent case is that of cholesterol, which, when incorporated into a lipid bilayer, has the ability to uncouple the two distinctly different lattice-melting and chain-melting processes [6,7]. Although some of the generic thermodynamics of such an interplay can be described by introducing new (somewhat artificial) lattice degrees of freedom [8], more realistic descriptions, especially of the translational degrees of freedom, are needed. It is one of the themes of the present work to explore this interplay by developing an appropriate description, in terms of both computer-simulation algorithms and microscopic interaction models, of the translational degrees of freedom and their coupling to the internal degrees of freedom.

A full microscopic (or first-principles) treatment of translational degrees of freedom would be ideal. Such a treatment is, however, very computationally demanding and severely limits any studies involving translational degrees of freedom [9]. Consequently, different approximation schemes are usually employed, depending on the scope of the study. For example, lattice-gas models are used to describe systems of interacting particles and gas-liquid transitions. In these models, the structure and the occupation of lattices account for the hard-core repulsion, the short-range nature of the molecular interactions, and the translational entropy. Despite the simplifications underlying these models, they capture the generic thermodynamic properties of gas-liquid transitions at which the full translational invariance of the system is preserved. It is necessary to invoke a different kind of approximation scheme, however, if breaking of translational symmetry is at issue, as is the case when solid-liquid transitions are considered.

In the present paper, we have developed a simple description based on the idea of representing microscopic spatial configurations of many-particle systems by configurations of a *randomly varying* triangular lattice. This *random-lattice* description is formulated in such a way that it is both adequate for describing collective phenomena manifesting the interplay between the internal (e.g., lipid chain conformational) and translational degrees of freedom in a class of two-dimensional systems and suitable for computer simulations. It is different from conventional lattice descriptions in that the lattice structure is dynamic (and semi-triangular): it can be seen as the result of "fluidizing" a *regular* triangular lattice through sampling over nonregular triangular lattice configurations with a fixed global topology. The global topology is here given by the Euler characteristics of the regular triangular lattice [10]. The phase space of the translational degrees of freedom, including both the part that respects the full translational symmetry, i.e., that corresponding to fluid phases, and the part that respects the broken symmetry, i.e., that corresponding to solid phases, should therefore be well approximated by this description. Our description is also different from conventional off-lattice descriptions in that it only provides a restricted phase space: those microscopic configurations that correspond to large density fluctuations on short length scales are effectively excluded. This approximation is, nevertheless, sufficient for describing condensed

fluid phases of systems of hard-core particles with short-range interactions.

Since our studies on the interplay between internal and translational degrees of freedom of many-particle systems have largely been motivated by the collective phenomena found in lipid-bilayer systems, we naturally see the purpose of developing the random-lattice description as being twofold: (i) to study the generic thermodynamic behavior of two-dimensional systems where the two types of degrees of freedom are present and coupled and (ii) to model this coupling in a way that is relevant to lipid-bilayer systems. To this end, we have chosen to study a series of three statistical mechanical models, which have different emphasis and levels of complexity in describing the microscopic interactions that govern the interplay of the two types of degrees of freedom. All three models are related to systems consisting of hard-core particles, each carrying a ''spin'' variable representing an internal degree of freedom. Interactions between particles are essentially spin-spin interactions, which are modeled in the spirit of the conventional Ising model defined on a regular lattice. Hence all three models are in essence Ising models defined on the random lattice.

Ising models defined on different types of 2D random lattices have been subject to considerable attention over the past years, in particular as model systems involving 2D gravity. Considerable progress was made by the finding of the exact solution for an Ising model on an unconstrained random triangular lattice [11]. It was shown that the critical behavior of this model is characterized by the critical exponents $\alpha = -1$ and $\beta = \frac{1}{2}$ [11], which are very different from those of the universality class of the standard two-dimensional Ising model ($\alpha = 0$ and $\beta = \frac{1}{8}$). The same results were also obtained numerically by Monte Carlo simulations [12]. A different approach was taken in a recent study of an Ising model on a dynamically generated lattice based on the spatial proximity of the particles in the plane [13]. In this study, spins were assigned to hard disks that were allowed to move in the plane, and in contrast to the random lattice considered here, the local lattice topology was not fixed. It was shown that, for condensed systems, the standard 2D Ising-model behavior was recovered, irrespective of the presence of full translational invariance [13]. As the hard-disk radius decreases with respect to the interaction range, the line of Ising critical (temperature) points was found to terminate at a tricritical-like point, and it was argued that the special critical behavior displayed by the Ising model on the unconstrained random triangular lattice [11] was again observed at this point. Beyond the tricritical-like point, the spin order-disorder transition becomes first order. In comparison with this work our studies always correspond to the condensed regime.

It should be noted that 2D random lattices also play a role in simulation studies of the shapes of fluid membranes, where the fluidity (or a certain type of randomness) of the lattice is crucial for the correct description of large-scale conformational properties of the membranes [14–16]. To a large extent the numerical dynamic-triangulation procedure discussed in this paper has been carried over from studies of fluid membrane conformations. In this respect our study bears some resemblance to a study of the mechanical properties of the spectrin network of the red-blood-cell membrane

by Boal, Seifert, and Zilker [17].

The paper is organized as follows. Section II gives an essential account of the random-lattice description in the context of the Metropolis Monte Carlo simulation algorithm. Some of the more technical issues are discussed in the Appendix. Section III describes in considerable detail the various two-dimensional models that we have studied. Section IV presents the simulation results obtained for the different models and our analysis of those results, along with discussions that rationalize the simulation results and underline the generic phenomenology of, and physical mechanisms underlying, the macroscopic coupling and decoupling between the translational and internal degrees of freedom. The comparison of some of the simulation results with a recent experimental observation of a new phase transition in lipid-bilayer systems is also given in this section. Section V concludes the paper with a brief reiteration of the work reported and a remark on possible further applications of the random-lattice-model approach we have taken.

II. RANDOM-LATTICE DESCRIPTION

In this section the random lattice is introduced as a basic representation of the translational degrees of freedom, upon which the specific microscopic models of Sec. III are constructed so as to take into account internal (spin) degrees of freedom and their coupling to the translational degrees of freedom. Furthermore, the implementation of the random lattice will be described and discussed as an integral part of the Monte Carlo simulation methods used in our study, to the extent that is necessary for understanding the essential features of the random-lattice description. Some of the more technical details of the implementation are relegated to the Appendix.

The translational degrees of freedom of a 2D many-particle system are conveniently represented by the planar coordinates (x,y) of the particles. A particle configuration is therefore given by $\{(x_n,y_n),n=1,\ldots,N\}$, where N is the total number of particles. When dealing with interactions between particles, the most important information required concerns the local environment of each individual particle, such as the distribution of other particles in its neighborhood and their distances to it. In conventional simulations that explicitly deal with the translational degrees of freedom, it is usually one of the most time-consuming steps to obtain and update this information from the microscopic configurations. In this section, we describe an algorithm that handles structural information in a manner that is distinctly different from conventional off-lattice algorithms and at the same time achieves high computational efficiency.

A. Algorithm

Our algorithm is a version of the dynamic-triangulation algorithm used for modeling fluid membranes [18], adapted to 2D planar systems of many particles. The algorithm performs two essential tasks: (i) it generates the phase space associated with the translational degrees of freedom and (ii) it generates and retains a compact data structure that allows efficient access to structural information contained in each microscopic configuration. The data structure is based on triangulation of each spatial configuration of the particles.
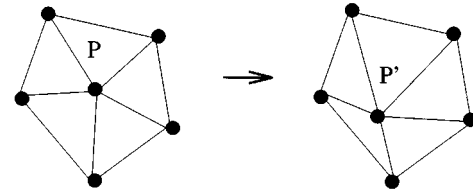

FIG. 1. Particle move. The hard disk at position P is moved to position P'.

This triangulation is implemented as follows. An ordered configuration in which the particles are positioned on a regular triangular lattice is used as an initial state in which each site is linked to its six nearest neighbors by tethers. The lattice configuration is then represented by a network of tethers forming triangles; the term ''triangulation'' refers to this representation. The phase (or configuration) space can then be explored through a random updating (or stochastic evolution) of configurations of the lattice, which consists of three steps to be described in the following subsections. All these steps are subject to the standard Metropolis Monte Carlo (MC) acceptance criterion [19]. According to this criterion, the probability of accepting an attempted move from a configuration i to a configuration f is given by $\min(1,P_{if})$, where

$$P_{if}=\exp(-\Delta H/k_B T). \qquad (1)$$

H is an effective Hamiltonian describing microscopic interactions, as given by specific models, $\Delta H=H_f-H_i$, and k_B is the Boltzmann constant. A detailed description of the microscopic models studied in the paper will be presented in Sec. III. We note, however, that in all the models, the short-range repulsion between particles is modeled as a hard-core repulsion. Each particle is then considered as a hard disk of diameter d and every site on the random lattice is occupied by such a hard-core particle.

1. Particle moves

The first step in the MC updating procedure is the ''particle move,'' which is illustrated in Fig. 1. A particle is chosen at random and its center is subject to a random displacement $(\delta x,\delta y)$, where

$$\delta x=(2\zeta_x-1)\delta r_{\max},$$
$$\delta y=(2\zeta_y-1)\delta r_{\max}. \qquad (2)$$

ζ_x and ζ_y are random numbers, $0\leqslant\zeta_{x(y)}\leqslant1$. The value of $\delta r_{\max}$ is adjusted during the simulations so that approximately 25% of the moves are accepted. Moves that would result in an overlap of hard disks are always rejected. Another constraint is that the length of every tether is not allowed to exceed a maximum value $d_{\max}$.

2. Link flip

The second step is referred to as the ''link flip.'' In each configuration of the random lattice, each tether (or link) is one diagonal of a quadrilateral formed by the two adjacent triangles. In the link flip, a tether is chosen at random; this
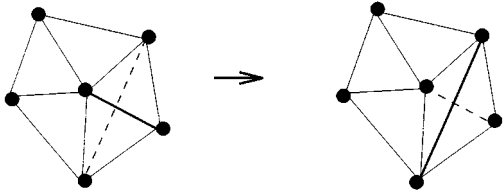
FIG. 2. Link flip. A tether (shown as thick line) is replaced by another tether along the diagonal (dashed line) provided that the length of the replacement does not exceed d_{max}.

tether is either replaced by a tether along the other diagonal of the quadrilateral if the length of the replacement does not exceed d_{max} or kept otherwise. A link flip is illustrated schematically in Fig. 2.

The combination of the particle move and the link flip makes the lattice ''dynamic'' (or random) in the sense that its configuration evolves through stochastic variations in both the local connectivity of the lattice and the real-space coordinates of the particles. This ensures both particle diffusion across the whole system and fluctuations in local particle distribution, as required in any description of the translational degrees of freedom.

In this part of the algorithm, the constraint of maximum tether length is employed. The reason for employing this constraint is that the main data structure used in our algorithm describes the position of each individual particle relative to its tethered neighbors. This is referred to as the ''link structure.'' When the tether length is bounded, a one-to-one mapping can be efficiently established from a given link structure to a nearest-neighbor structure. One may expect that this constraint prevents the algorithm from accessing the *entire* phase space spanned by the 2D translational degrees of freedom since those microscopic configurations that correspond to strong short-length-scale fluctuations in the particle density are not compatible with the constraint. To address this issue, we have revisited, using our algorithm, the system of hard disks, as will be described in Sec. IV.

3. Change of system size

In the constant N-P-T ensemble used here it is necessary to allow the area of the system to fluctuate. In our simulations this is achieved via a third step in the MC procedure: a random uniform expansion or contraction of the whole system. In this step, a random change in the size of the system is generated by rescaling the length as

$$\delta L = (2\zeta - 1)\delta L_{max}, \qquad (3)$$

where ζ is a random number, $0 \leq \zeta \leq 1$, and the coordinates of all particles and the maximum tether length d_{max} are rescaled accordingly. d_{max} is rescaled in order to allow for a significant density decrease for low values for the lateral pressure [20]. If the distance between any two particles after the rescaling is smaller than the hard-disk diameter, the change is always rejected. The maximum possible size change δL_{max}, is adjusted during the simulation to give an acceptance ratio of about 50%.

In this MC updating procedure for a change of system size, the probability of accepting a move from a state with an area $A_i = L^2$ to a state with an area $A_f = (L + \delta L)^2$ is determined by $\min(1, P_{if})$, where P_{if} is given by Eq. (1) with H defined as $H = H_{model} + H_{HD}$. H_{model} is the model-dependent microscopic Hamiltonian describing the interactions between the particles and

$$H_{HD} = PA - k_B TN \ln A. \qquad (4)$$

The first term in H_{HD} represents the energy associated with the lateral pressure P and the second term reflects the degeneracy of a microscopic configuration of $2N$ translational degrees of freedom.

In our simulation, a MC update of the random lattice is defined as an attempt to move every particle, flip every tether in the lattice, and ten attempts to change the system size. A sufficiently large number of the simulation steps then generates a configuration (phase) space that is characteristic of the translational degrees of freedom of the system. It is important to emphasize that the given Hamiltonian H_{model} describing the microscopic interactions between particles is included in the acceptance criterion Eq. (1) for all of the three steps in the MC update for the random lattice.

III. MICROSCOPIC HAMILTONIANS

In this section we present three different models of increasing complexity, referred to in this paper as models I, II, and III, where the random-lattice description of the noninteracting hard-disk particle system is extended to include internal degrees of freedom and microscopic interactions that couple the internal degrees of freedom to the translational degrees of freedom. In essence all three models are variants of the Ising model defined on a regular lattice.

A. Models I and II: Ising models on the random lattice

The 2D spin-1/2 Ising model defined on a regular triangular lattice has a continuous phase transition from a high-temperature paramagnetic (spin-disordered) phase to a low-temperature ferromagnetic (spin-ordered) phase at a critical temperature $k_B T_C / J_0 = 3.641$, where J_0 is the exchange interaction between nearest-neighbor spins. We have extended this standard model in two ways. Our first extension, which will be referred to as model I, is to associate a spin with each hard-core particle on the random lattice. Nearest-neighbor particles are connected by tethers and interact through the usual Ising spin-spin-exchange interaction. This leads to a *random* Ising model in which the number of nearest neighbors is a fluctuating quantity. In this model, the characteristic interaction range is set by the particle density of the system, which in turn is controlled by the external pressure P and the translational and spin degrees of freedom are only coupled by the *fluctuating* local connectivity (or the number of nearest neighbors) of the random lattice. For later reference, we write down the microscopic interaction Hamiltonian used in our simulation,

$$H_I = -J_0 \sum_{\langle i < j \rangle} S_i S_j, \qquad (5)$$

where $\langle i < j \rangle$ denotes a sum over nearest neighbors connected by tethers and $S_i = \pm 1$.

In the second extension of the standard Ising model, which will be referred to as model II, we have modified the above model in Eq. (5) by introducing a spin-spin interaction that is *distance dependent*: the tethered spins only interact if they are within a certain distance R_0 of each other. The random-lattice Hamiltonian is then given by

$$H_{\mathrm{II}} = -J_0 \sum_{\substack{\langle i < j \rangle \\ R_{ij} < R_0}} S_i S_j, \tag{6}$$

where $\langle i < j \rangle$ again denotes a sum over all possible nearest neighbors and R_{ij} is the distance between spins S_i and S_j. Hence, in this case, R_0 sets the range of interaction. The fact that the density of the system sets another length scale leads to a different type of coupling between the spin and the translational degrees of freedom.

With these two models, we can address the basic issue of how and to what extent different types of microscopic coupling between the internal and translational degrees of freedom manifest themselves in the macroscopic thermodynamic behavior of the systems and understand and underline the generic physics associated with such coupling. Ising spin transitions in these models will be of particular interest, as the classical understanding of the critical transition in the Ising model defined on a regular lattice provides an essential framework of reference, with respect to which effects arising from the interplay between the two types of degrees of freedom can be mapped out.

B. Model III: The Doniach model on the random lattice— A model for lipid bilayers

Model III is, in principle, an Ising model similar to those introduced above, but with a basic difference that one of the spin states is assigned an internal degeneracy larger than one. This model is inspired by a *regular-lattice* model proposed by Doniach [4] to describe the essential thermodynamic properties of lipid bilayers, in particular the main transition, that are primarily associated with the conformational degrees of freedom of lipid chains in a planar array. Doniach's model uses two states to represent the lipid-chain conformation. One state, the ''ordered'' state (denoted $S_i = 1$), has zero internal (conformational) energy ($E_o = 0$) and is nondegenerate ($D_o = 1$), characteristic of the chain conformational state of lipid molecules in the gel phase. The other state, the ''disordered'' state (denoted $S_i = -1$), has a high internal energy E_d (corresponding to the excitation energy associated with a conformational change) and a large degeneracy $D_d \gg 1$ (representing the large number of possible chain conformations that have the same value of E_d) characteristic of the chain conformation of lipid molecules in the liquid-crystalline (fluid) phase. Each chain occupies a site on a regular triangular lattice and each state is assigned a cross-sectional area A_o or A_d corresponding to the average area occupied by chains in the ordered and the disordered state, respectively. This regular-lattice model is described by the Hamiltonian

$$H_D = H_0 + V_{\mathrm{int}}^{(1)} + P \sum_i \left\{ A_d \left(\frac{1 - S_i}{2} \right) + A_o \left(\frac{1 + S_i}{2} \right) \right\}, \tag{7}$$

where

$$H_0 = \sum_i E_d \left(\frac{1 - S_i}{2} \right) \tag{8}$$

and

$$V_{\mathrm{int}}^{(1)} = -\frac{J_0}{4} \sum_{\langle i < j \rangle} (1 + S_i)(1 + S_j), \tag{9}$$

with $\langle i < j \rangle$ denoting a sum over nearest neighbors. In this case, P plays the role of an internal interfacial pressure that provides the lateral stabilizing force controlled mainly by the hydrophobic effect at the lipid-water interface. H_0 describes the chain internal energy. $V_{\mathrm{int}}^{(1)}$ models the chain-chain interaction, which (somewhat arbitrarily) is taken to be nonzero only if a chain and its neighbor are both in the ordered state. Obviously, this is an approximation to the fact that the interchain forces are diminished when either or both of the neighboring chains are in the disordered state, but it is formally equivalent to setting the relative energy scales of the Hamiltonian. The third term in Eq. (7) represents the energy cost of stabilizing the lipid system against lateral expansion.

It is straightforward to determine the thermodynamic behavior of this model [4], which is isomorphic to an Ising model in a temperature-dependent field, i.e.,

$$H_D = E_0 - \frac{J_0}{4} \sum_{\langle i < j \rangle} S_i S_j + \sum_i h_{\mathrm{eff}}(T) S_i, \tag{10}$$

where E_0 is a trivial constant, $h_{\mathrm{eff}}(T) = -\frac{1}{2}[E_d + (z/2)J_0 + P\Delta A - k_B T \ln D_d]$, $\Delta A = A_d - A_o$, and z is the coordination number of the lattice ($z = 6$ for the regular triangular lattice). At low temperatures the effective field ''prefers'' the chains to be in the ordered state. As T increases, the system crosses over from the ordered state to the disordered state at a temperature T_m determined by

$$h_{\mathrm{eff}}(T_m) = 0, \tag{11}$$

provided that T_m is less than the critical temperature T_C of the standard Ising model. This transition is effectively a field-induced transition below the critical temperature of the standard Ising model and is therefore a first-order transition usually referred to as the ''chain-melting'' transition.

While the Doniach lattice model includes the most essential physics associated with the lipid-chain conformational degrees of freedom, it ignores the translational degrees of freedom. We therefore propose an extension of the Doniach model to account for the interplay between the conformational and the translational degrees of freedom in the simplest way: the translational degrees of freedom of lipid chains are governed by interchain interactions that depend on the conformational states of the interacting chains. This extended model, which we refer to as model III, is described by the *random-lattice* Hamiltonian

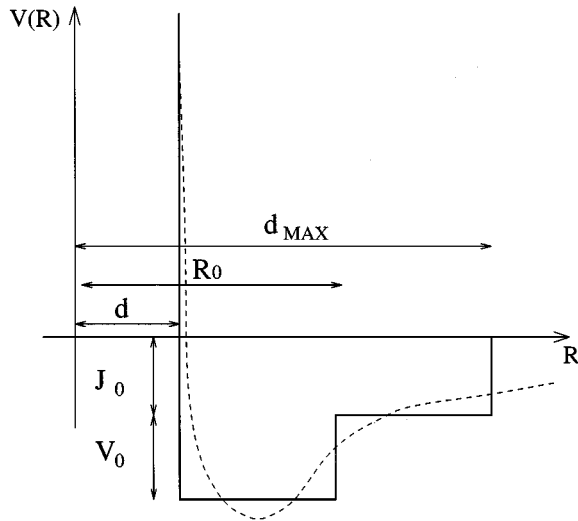$$H_{\mathrm{III}} = H_0 + V_{\mathrm{int}}^{(1)} + V_{\mathrm{int}}^{(2)} + PA, \tag{12}$$

FIG. 3. Schematic illustration of the interaction potential $V(R)$ in model III. It consists of a sum of a hard-disk potential and two square-well potentials. The hard-disk radius is d and the range and strength of the square-well potentials are (d_{max}, R_0) and (J_0, V_0), respectively. The dashed line illustrates a Lennard-Jones-like potential, to which the model potential is an approximation.

where

$$V_{int}^{(2)} = \frac{1}{4} \sum_{\langle i<j \rangle} V(|R_i - R_j|)(1 + S_i)(1 + S_j) \qquad (13)$$

and A is the total area of the system. $V(R)$ in Eq. (13) is a square-well attractive potential of depth V_0 and range R_0. $V_{int}^{(1)}$ and $V_{int}^{(2)}$ together provide an approximation to the attractive intermolecular interaction between any two chains in the conformationally ordered state. The sum of the hard-core potential and the two square-well potentials $V_{int}^{(1)}$ and $V_{int}^{(2)}$ constitutes an approximation to a standard intermolecular potential of the Lennard-Jones type, as schematically illustrated in Fig. 3. By analogy with the Doniach lattice model, the effective interaction between any two chains in model III is taken to be zero if either one or both of the chains are in the conformationally disordered state. The square-well potential described by R_0 and V_0 controls the minimum of the potential and hence the lattice parameter of the crystalline (solid) phase. The tail of the potential extending beyond R_0 permits a possible decoupling between the two melting (or order-disorder) processes associated with the translational and conformational degrees of freedom. This model is a minimal model in the sense that it contains only the most essential physics required to model the coupling between translational and internal degrees of freedom in lipid-bilayer systems.

The fundamental difference between model III and the lattice model of Doniach is that each chain in model III is allowed to have a varying number of nearest neighbors and varying distances from its neighbors. Furthermore, the chains are allowed to diffuse through the whole system, as the essential manifestation of translational invariance of the system. The two sets of degrees of freedom are thus coupled in a natural way through the intermolecular interactions. One

may expect that this model displays different types of thermodynamic behavior, depending on the strength of this coupling.

IV. SIMULATION RESULTS AND DISCUSSION

Before proceeding to presenting the numerical results obtained from the simulation studies of the models described in the preceding section, we first give an outline of the simulations themselves. All simulations were initialized using a state where the lattice configuration was crystalline (regular triangular) and the internal degrees of freedom were disordered. This initial configuration was then equilibrated by the Metropolis Monte Carlo algorithm to a high-temperature state with disorder in both the translational and internal degrees of freedom. Equilibrium states at lower temperatures were reached by cooling down from the high-temperature state in small temperature steps. In each of the cooling steps, a number of Monte Carlo updating steps [Monte Carlo steps per particle (MCS)] were discarded before the measurement of equilibrium thermodynamic quantities of the system was started. The number of MCS used to reach the equilibrium high-temperature state was between 30 000 and 50 000. The number of MCS discarded in the subsequent temperature steps was between 10 000 and 25 000. The measurement of various thermodynamic quantities was performed over a simulation period of 30 000–50 000 MCS. Among the calculated quantities are the enthalpy, the area, and the spin order parameter (the magnetization) per particle. Also calculated were the corresponding thermodynamic response functions, the isobaric specific heat per particle C_P, the area compressibility K, and the (spin) susceptibility per particle χ, which can be expressed by the fluctuation-dissipation theorem as

$$C_P = \frac{\langle H^2 \rangle - \langle H \rangle^2}{N k_B T^2}, \qquad (14)$$

$$\chi = \frac{\langle M^2 \rangle - \langle M \rangle^2}{N k_B T}, \qquad (15)$$

$$K = \frac{\langle A^2 \rangle - \langle A \rangle^2}{k_B T \langle A \rangle}, \qquad (16)$$

where H is the model Hamiltonian, M the total spin order parameter, A the total area of the system, and N the total number of particles. Signatures of thermodynamic singularities (or phase transitions) were identified from these measured equilibrium quantities. The phase behavior of each model was thereby determined.

In the analysis of the simulation data for the 2D liquid-solid transition we have, to a certain extent, used the histogram method of Ferrenberg and Swendsen [21,22]. Using this method we can extract a free-energy-like function from the Monte Carlo simulation data. Close to the lattice-melting transition point this free-energy function has a well-defined double-well structure. The transition temperature can thus be determined by using the standard technique of reweighting [21], and an estimate of the transition enthalpy ($\Delta \langle H \rangle$) can be obtained from the position of the two equilibrium minima of the free-energy function. We are, however, fully aware

that these estimates are associated with quite substantial error bars due to the lone Monte Carlo correlation time for the 2D system [23] and it is therefore difficult to draw definite conclusions about the nature of the fluid-solid transition from our simulations.

The presentation of the simulation results falls naturally into three parts. The first part contains a short summary of the results of our reexamination of the hard-disk system; the second part gives the results of the simulation study of the Ising models I and II; and the final part describes the results for the extended Doniach model, model III. Each part of the presentation is followed by a discussion of the generic physics entailed in the results.

A. Hard-disk system

As we noted in Sec. II, our random-lattice algorithm provides only an approximate description of the 2D translational degrees of freedom. The approximation is mainly related to the use of the constraint of maximum tether length in the algorithm, which to some extent prevents the algorithm from accessing the *entire* phase space spanned by the translational degrees of freedom. In order to assess the validity of this approximation, we have revisited the system of noninteracting hard disks by studying the solid-liquid transition in this system in the presence of our constraint. This solid-liquid transition is solely driven by the configurational entropy associated with the 2D translational degrees of freedom. Moreover, a recent simulation study by Lee and Strandburg using a full off-lattice algorithm [24] provides quantitative information on the transitional properties and presents numerical evidence that the transition is of first order (although this subject still remains a contentious issue). A numerical study of this system using our random-lattice algorithm therefore allows us to assess quantitatively any restrictive effect that the constraint may have on the representation of the translational degrees of freedom. We expect that, once the constraint is effectively removed by allowing a large value for the maximum tether length, our algorithm should lead to results that are consistent with those obtained by using the full off-lattice algorithm [24,25].

In the following, we give a short summary of the results for our study of the hard-disk system with the random-lattice algorithm. A hard-disk system with $N = L^2 = 12^2$ particles was simulated for two cases with respect to the constraint of the maximum tether length. In the first case, a strong constraint was employed in the algorithm; in the second case, this constraint was relaxed. In the case of the relaxed constraint the algorithm was modified to include a cell-list structure to facilitate a fast check of steric interactions between neighboring hard disks [26]. During the simulations the structure factor of the system was calculated as

$$S(\vec{k}) = \left\langle \sum_i e^{i\vec{R}_i \cdot \vec{k}} \right\rangle, \qquad (17)$$

where $\vec{R}_i$ is a two-dimensional vector giving the position of disk i and $\langle \ \rangle$ denotes a thermal average. In Fig. 4 $S(\vec{k})$ is shown for different values of the reduced lateral pressure $P^* = Pd^2/k_BT$, where d is the hard-disk diameter. For the constrained case, there is a clear change in lateral order as

the value of the reduced pressure is changed from 8.75 to 9.75, as indicated in Figs. 4(a) and 4(b). Using the reweighting histogram method [21], we have found the position of the transition to be at $P^* = 9.15$. We have also estimated the change in the average area per molecule across the transition to be $\Delta a = a_l - a_s \simeq 0.014$, where $a_{s(l)} = (A_{s(l)}/d^2N)(2/\sqrt{3})$ and $A_{s(l)}$ is the total area of the solid (liquid) phase. As the constraint on the tether length is relaxed, the lattice-melting event shifts to a value of the reduced pressure between 8.25 and 8.75, as illustrated in Figs. 4(c) and 4(d). Again, by using the reweighting histogram method, the position of the solid-fluid transition is found to be located to be at $P^* = 8.55$ and the value of the area change across the transition is estimated to be $\Delta a \simeq 0.052$.

These results demonstrate that, as the constraint is relaxed, our simulation data converge toward the results for P^* obtained from other off-lattice studies of the hard-disk system [24]. For example, the work reported in Ref. [24] estimates that $P^* \simeq 8.0$ and $\Delta a \approx 0.05$ in the limit of $L \rightarrow \infty$. Our results also show that the essential characteristics of the transition remain largely intact in the random-lattice algorithm, although imposing the constraint of maximum tether length to a certain extent results in artificial changes in transition quantities, such as the small shift in the transition pressure. However, since we have not in the present work performed a systematic finite-size analysis or a detailed study of the relaxation times [25], we will not make a closer comparison with the results from other theoretical work on the hard-disk melting transition.

It is, however, necessary for the discussion in the rest of the paper that we make a remark on the nature of solid-liquid transitions in two-dimensional systems (or 2D melting). The nature of 2D melting transitions has been a focal point of numerous statistical-mechanical studies of two-dimensional systems for the past two decades [27,28]. Two scenarios have been presented and discussed. Halperin and Nelson, and Young [29] developed the basic idea of Kosterlitz and Thouless, and Berenzinskii [30] and proposed the scenario that the 2D solid-liquid transition can proceed via two continuous (second-order) transitions corresponding, respectively, to dissociation of dislocations (the solid-hexatic transition) and dissociation of disclinations (the hexatic-liquid transition). A single conventional first-order transition is the other possible scenario. Despite the significant amount of effort devoted to resolve the issue, no final consensus has been reached. While most Monte Carlo simulations suggest a first-order 2D melting [24], others suggest a one-stage continuous transition [25]. In the work presented in this paper, where we consider the effects of coupling the translational degrees of freedom to internal degrees of freedom of the particles, we are inevitably confronted with this issue. Unfortunately, by studying a more complex model we may not be able to provide any new information on the true nature of the 2D melting transition. However, for all practical purposes and without any restriction on the results we report here we can consider that the melting is a first-order transition. In fact, for the models examined in this paper all the simulation data obtained for the solid-liquid transition are consistent with a first-order transition.
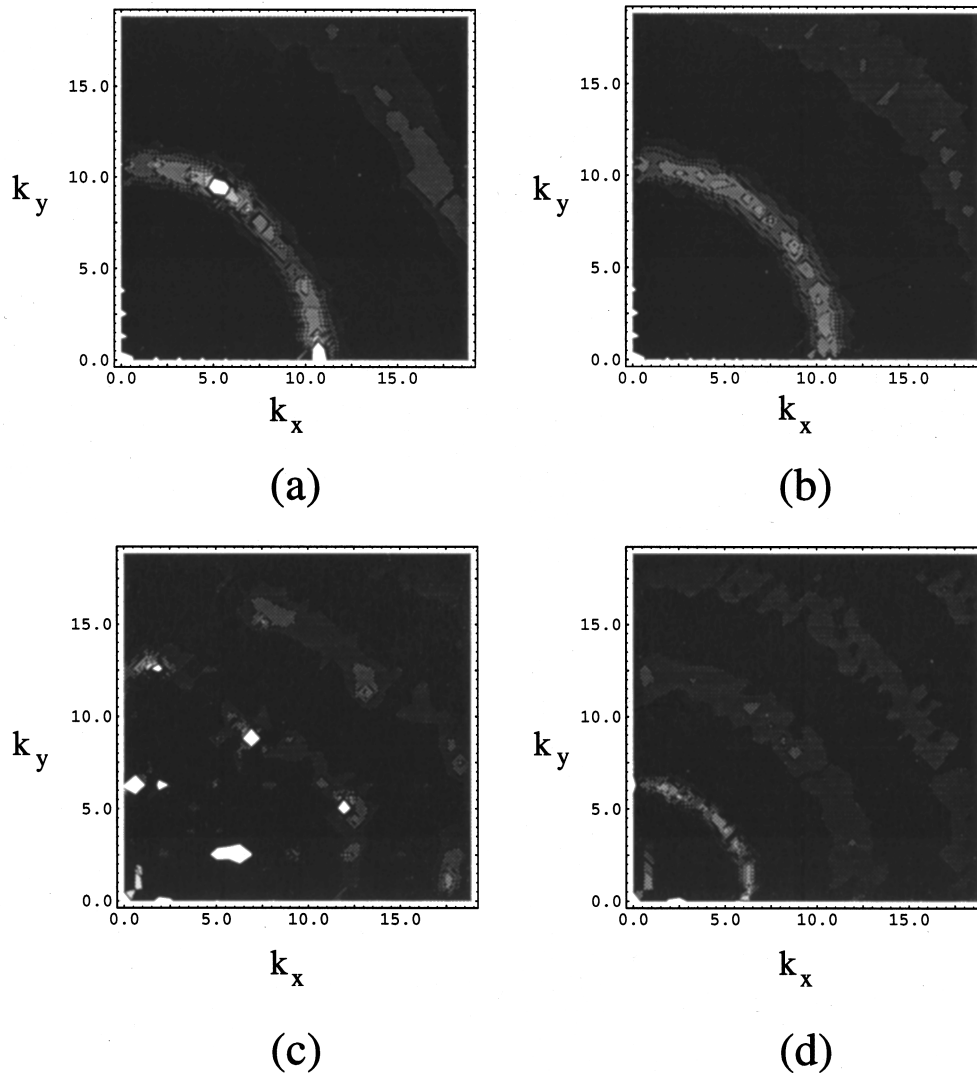
(a)

(b)

(c)

(d)

FIG. 4. Contour plot of the structure factor $S(\vec{k})$ in the (k_x, k_y) plane calculated for the hard-disk system of size $N = 144$. In (a) and (b) $\langle d_{max} \rangle \simeq 1.73d$ and $d = 0.6$. Here $\langle \ \rangle$ denotes a thermal average. In (c) and (d) $\langle d_{max} \rangle \simeq 7d$ and $d = 1.0$. The value of the reduced lateral pressure is (a) $P^* = 9.75$, (b) 8.75, (c) 8.75, and (d) 8.25. The position of the first Bragg peak is at a k value of $2\pi/d$, which for system (a) corresponds to $|k| \simeq 10.5$ and (c) $|k| \simeq 6.28$.

B. Ising model I and Ising model II on the random lattice

Ising models I and II were formulated to describe two-dimensional systems where both internal (spin) and translational degrees of freedom are present and are coupled through microscopic interactions. Consequently, characterization of the phase behavior of these model systems requires knowledge of the macroscopic behavior of *both* types of degrees of freedom. As the macroscopic behavior of the translational degrees of freedom is described as either solid or liquid and that of the spin degrees of freedom is characterized as either (spin) ordered or (spin) disordered, each model system can, in principle, have four different phases: a solid-ordered (SO) phase, a solid-disordered (SD) phase, a liquid-ordered (LO) phase, and finally a liquid-disordered (LD) phase. We will use this terminology below in our description of the phase behavior of the three models of Sec. III. Our simulation study of the models concentrates on identifying these possible phases in parameter spaces of the models, locating the boundaries between the different phases and characterizing the nature of the thermodynamic singularities associated with the phase boundaries.

For Ising model I, a convenient choice for the parameter space is given by a reduced (or dimensionless) lateral pressure, defined as Pd^2/J_0, and a scaled temperature T/T_C, where T_C is the critical temperature of the spin transition in the Ising model on the regular triangular lattice. The simulation study of Ising model I was performed for a range of values of the (reduced) lateral pressure and the (reduced) temperature. The results show that the four phases described above are indeed all present in the region of the parameter space explored. Moreover, the phase boundaries separating these four phases are simply two intersecting lines: one line is predominantly controlled by the solid-liquid thermodynamic singularity and is considered to be a first-order line, and will be termed as the ''lattice-melting'' transition; the second line is mainly associated with a critical order-disorder transition of the spin system. Specifically, the high-temperature phase is the LD phase, the low-temperature
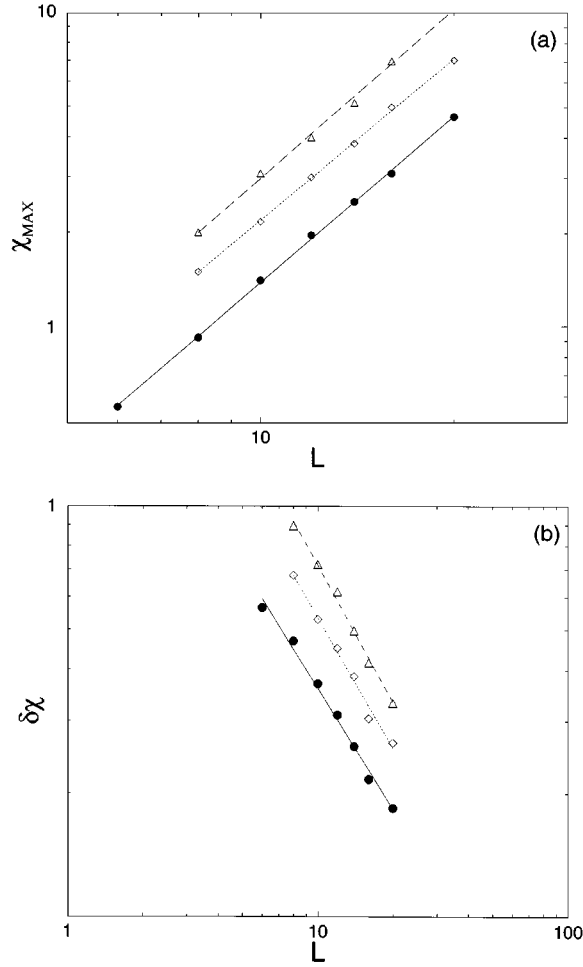
FIG. 5. Finite-size scaling plots for Ising model I in the cases of three different values of Pd^2/J_0. (a) $\chi_{\max} \sim L^{\gamma/\nu}$ and (b) $\delta\chi \sim L^{-1/\nu}$. The upper curve ($\triangle$) corresponds to $Pd^2/J_0 = 10.0$, the middle curve ($\diamond$) to $Pd^2/J_0 = 30.0$, and the lower curve ($\bullet$) to $Pd^2/J_0 = 50.0$. For clarity the three curves are shifted along the vertical axis. (a) The values for the ratio of the exponents γ and ν for the three curves are 1.76 ± 0.02, 1.73 ± 0.02, and 1.78 ± 0.05, respectively. (b) The corresponding values of the exponent $1/\nu$ are 0.98 ± 0.04, 1.06 ± 0.06, and 1.09 ± 0.05, respectively.

phase is the SO phase, the low-pressure, intermediate-temperature phase is the LO, and finally the high-pressure, intermediate-temperature phase is the SD phase. For low pressures, e.g., $Pd^2/J_0 = 10.0$, the critical Ising spin transition has a higher temperature than the lattice-melting transition. As the pressure increases, the temperature difference between the two transitions decreases. At the point of intersection, where $Pd^2/J_0 = 30.0$, the two transitions coincide in temperature. For higher pressures, e.g., $Pd^2/J_0 = 50.0$, this ordering in temperature is reversed and the lattice-melting transition actually has a higher temperature than the Ising spin transition.

In order to investigate the critical behavior of the Ising spin transition in this model and to compare it to that of the regular-lattice Ising model, a finite-size scaling analysis of the simulation data for this transition was carried out. Figure 5 shows the results of the analysis of three sets of simulation data obtained for three different values of the lateral pres-

sure, $Pd^2/J_0 = 10.0$, 30.0, and 50.0, as also cited in the preceding paragraph. The total number of particles $N=L^2$ varied in the finite-size scaling analysis from 64 to 400. The finite-size scaling theory for continuous transitions leads to the following hypothesis for scaling relations of thermodynamic response functions with the system size L [31]:

$$\chi_{\max} \sim L^{\gamma/\nu}, \tag{18}$$

$$C_{P,\max} \sim L^{\alpha/\nu}, \tag{19}$$

$$\delta\chi \sim L^{-1/\nu}, \tag{20}$$

where $\chi_{\max}$ and $C_{P,\max}$ are the peak values of the spin susceptibility and the specific heat for the finite-size system and $\delta\chi$ is the half width of the spin susceptibility curve. In our analysis, the value of $\chi_{\max}$ ($C_{P,\max}$) was taken as an average of the maximum value of the susceptibility (the specific heat) over five different simulation runs. The value of $\delta\chi$ was taken as the average value of the half width over the five different χ curves [32]. As it is clear from Fig. 5, the critical exponents γ and ν found from the finite-size scaling analysis are, within the statistical error of the calculations, all consistent with those of the 2D regular-lattice Ising model ($\gamma = 7/4, \nu = 1$) [33]. It would be much more demanding to perform a finite-size scaling analysis of the specific heat (data not shown) because of the very weak singularity and the influence of a nonsingular term in C_P, which cannot be neglected at finite L. However, the C_P data for the larger system sizes shows a fairly weak dependence of $C_{P,\max}(L)$ on L, indicative of a small specific-heat exponent $\alpha \sim 0$, consistent with the logarithmic singularity ($\alpha = 0$) associated with the regular-lattice Ising critical behavior. We thus conclude that, within the range of lateral-pressure values studied in our simulation, the Ising model I defined on the *dynamic* random lattice belongs to the same universality class as the regular-lattice Ising model.

Overall, the simulation study of Ising model I shows that there is no significant macroscopic manifestation of the microscopic coupling between the spin and the translational degrees of freedom. This observation can be rationalized as follows. In this model, the particle-particle interaction has no distance dependence and the microscopic coupling between the two types of degrees of freedom is only facilitated through the fluctuating local connectivity of the lattice. In the condensed systems considered here, not only are the fluctuations in the local connectivity of the lattice small, but there is also no change in the macroscopic value of the local connectivity as the systems change from solid to liquid state. In other words, the microscopic coupling does not give rise to any strong coupling between the macroscopic behavior of the spin and the translational degrees of freedom that could couple or alter the characteristics of their corresponding thermodynamic singularities.

Ising model II describes a more complex type of microscopic coupling between the spin and the translational degrees of freedom: in addition to the coupling through the fluctuating local connectivity, there is also coupling through the distance-dependent (R_0) spin-spin interaction. The emphasis of our study of this model is to investigate whether the
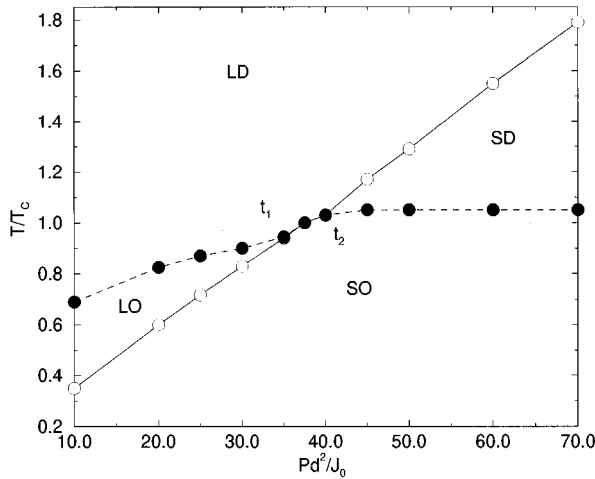
FIG. 6. Phase diagram for Ising model II for $R_0/d=1.41$. The dashed phase boundary line ($\bullet$) corresponds to the critical Ising-like transitions from a spin-ordered (SO) to a spin-disordered (SO) phase. The solid boundary line ($\circ$) corresponds to the first-order lattice-melting transition from a solid phase to a liquid phase. t_1 and t_2 are the two critical end points described in the text. Between the two critical end points the spin order-disorder singularity is coupled to the lattice melting and is of first order.

more complex microscopic coupling will lead to intricate coupling at the macroscopic level and, in turn, to more complex phase behavior.

Indeed, Ising model II was found to have more complex phase behavior, in particular with respect to the coupling of the degrees of freedom at the macroscopic level. Displayed in Fig. 6 is the phase diagram for the model, given in the same parameter space of the reduced pressure and the scaled temperature for a fixed $R_0/d=1.41$. The phase diagram was obtained from simulation data and our analysis of that data. Again, as in Ising model I, the four principal phases are all present and the remnant of the phase diagram of Ising model I can be seen in the low-pressure and high-pressure regions of the parameter space, where the lattice-melting transition and the critical spin transition are decoupled and where LO and SD phases intervene between the SO and the LD phases. However, the phase boundaries separating these phases no longer consist of two intersecting lines alone: a new phase boundary directly separating the SO and the LD phases is now present, as indicated by the solid line between the two special points t_1 and t_2. These two points are actually critical end points (see below) and their locations ($Pd^2/J_0|_{t_1}=35$, $T/T_C|_{t_1}=0.945$) and ($Pd^2/J_0|_{t_2}=40$, $T/T_C|_{t_2}=1.035$), as indicated in the phase diagram, are only estimates (which include finite-size effects) [34]. Along this phase boundary, which is of first order, the translational degrees of freedom override the spin degrees of freedom and the lattice-melting transition preempts the critical spin transition, leading to a first-order singularity also in the spin order parameter.

Presented in Figs. 7–9 is a collection of simulation data obtained for Ising model II, which corroborates the phase diagram. Figure 7(a) shows the change of area (per molecule) with temperature for a set of values of pressure that cover the parameter range we have investigated. An abrupt (effectively discontinuous) change in the area takes place at a
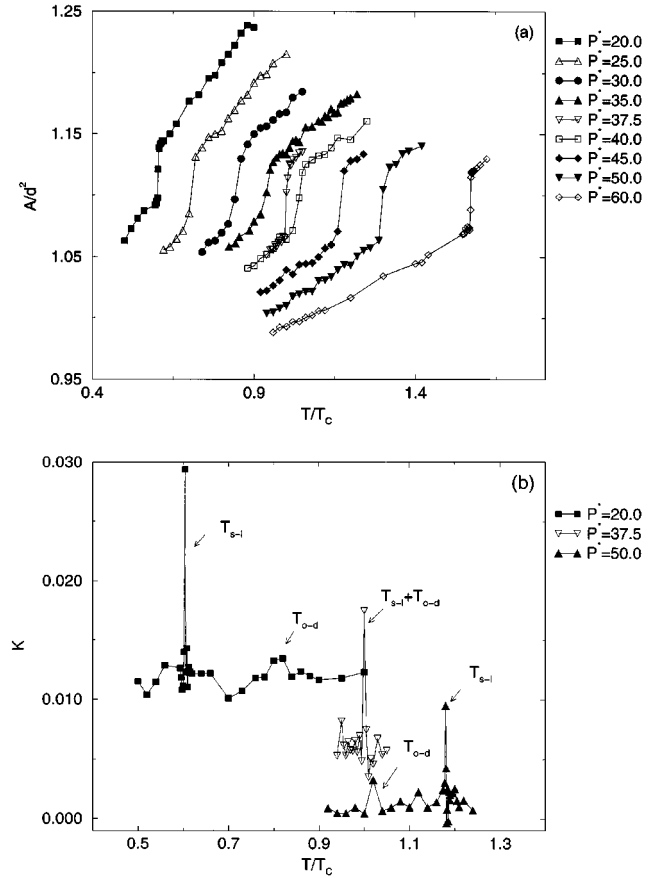

FIG. 7. (a) Area A per particle and (b) the corresponding area compressibility K of Ising model II for different values of the lateral pressure $P^*=Pd^2/J_0$. The system size is $N=256$ and $R_0/d=1.41$. The temperature is given in units of the critical temperature T_C of the regular lattice Ising model. For clarity, the K curves are shifted along the vertical axis by multiples of 0.005.

specific (pressure-dependent) temperature for all the pressure values considered. The corresponding response function, the area compressibility K given in Fig. 7(b), displays the signature of the same singularity. These data are taken as the evidence for the first-order lattice melting transition. The critical spin order-disorder transition, existing in both the low-pressure ($P<P_{t_1}$) and the high-pressure ($P>P_{t_2}$) regions, is identified principally from the simulation data such as those shown in Fig. 8. The temperature dependence of the spin order parameter is given in Fig. 8(a) for a set of pressure values. Both at low values and high values of the pressure, the spin order parameter varies steeply, but *continuously*, at a particular (pressure-dependent) temperature, concomitantly with the occurrence of a peak at the same temperature in the spin susceptibility function χ in Fig. 8(b). This particular temperature is thus determined for each value of the pressure, giving the location in the parameter space of the critical spin transition. As expected, the specific heat C_P, which carries information about energy fluctuations arising from fluctuations in both the translational and spin degrees of freedom, displays sharp peaks at both transitions, as Fig. 9 clearly demonstrates. The identification of the solid and liquid characteristic of the phases has also been confirmed by analysis of the structure factor $S(\vec{k})$ (data not shown). $S(\vec{k})$
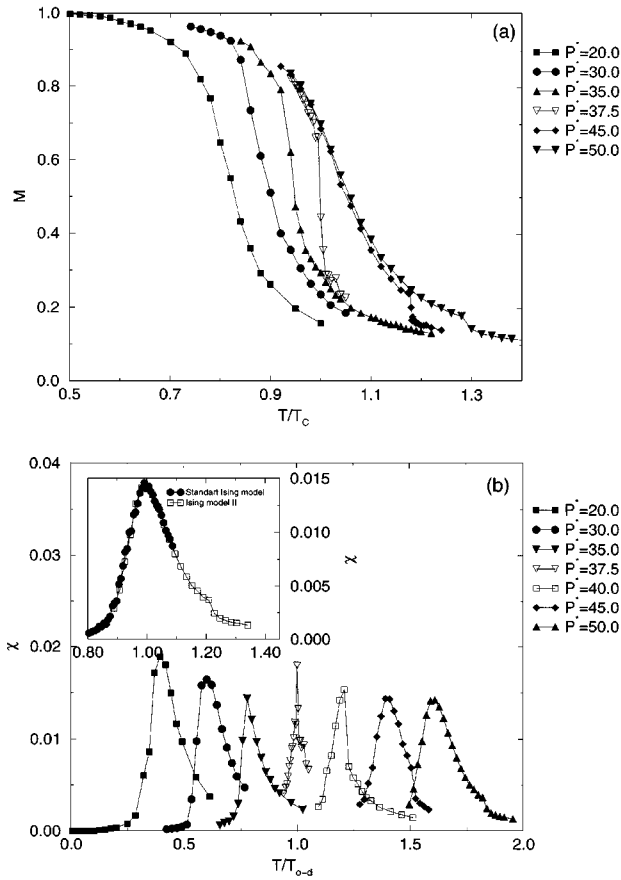
FIG. 8. (a) Spin order parameter M and (b) the corresponding susceptibility χ of Ising model II for different values of the lateral pressure $P^* = Pd^2/J_0$. The system size is $N = 256$ and $R_0/d = 1.41$. M is shown as a function of T/T_C, whereas χ is given as a function of T/T_{o-d}, where T_{o-d} is determined by the peak position of χ. For clarity the χ curves are shifted along the horizontal axis. The actual peak position for the different curves are $0.825T_C$, $0.89T_C$, $0.98T_C$, $1.00T_C$, $1.03T_C$, $1.05T_C$, and $1.05T_C$, respectively. The inset in (b) shows a comparison between χ of the regular-lattice Ising model and χ of Ising model II for $P^* = 50.0$.

has clear Bragg peaks in the solid phase and displays only diffuse rings in the liquid phase.

The simulation data suggests that the critical temperature of the spin transition separating the LO and the LD phases in the low-pressure region has an observable pressure dependence, whereas the temperature of the critical spin transition separating the SO and SD phases in the high-pressure region coincides with the critical temperature of the regular-lattice Ising model (as expected). In order to investigate the critical behavior of the spin transitions in more detail in both the low-pressure and the high-pressure regions, we have also performed finite-size scaling analysis of the simulation data on the spin susceptibility χ in the low-pressure region, based on the scaling hypothesis described in Eq. (18), and the result of the analysis is shown in Fig. 10. It is clear from this figure that the universal Ising critical behavior is unaltered by the fluctuations in the density (or local connectivity of the random lattice). On the high-pressure side of the critical end point t_2, both the universal and nonuniversal behavior of the critical transition is expected to be identical to that of the
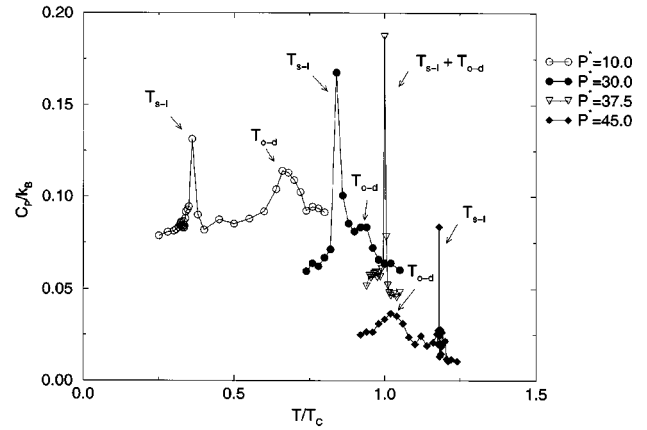

FIG. 9. Specific heat C_P per particle of Ising model II as a function of T/T_C for different values of the lateral pressure $P^* = Pd^2/J_0$. The system size is $N = 256$ and $R_0/d = 1.41$. For clarity the C_P curves are shifted along the vertical axis by multiples of 0.025. For low values of the lateral pressure P^* ($P^* = 10.0$ and $P^* = 30.0$) the temperature of the critical spin transition T_{o-d} is higher than the lattice-melting temperature T_{s-l}. At higher values of P^* ($P^* = 45.0$) T_{s-l} is higher than T_{o-d}. For intermediate values of P^* ($P^* = 37.5$) the two transitions are coupled and $T_{o-d} \simeq T_{s-l}$.

regular-lattice Ising model. This is confirmed by the data shown in the inset in Fig. 8(b), which demonstrate that, in this pressure region, the susceptibility fits perfectly in shape (as a function of T) to the susceptibility of the regular-lattice Ising model in the neighborhood of the critical temperature.

The phase boundary between the two special points t_1 and t_2 (see Fig. 6) distinguishes the phase behavior of Ising model II from that of Ising model I. It lies directly between the SO and LD phases. The first-order nature of this phase transition is indicated by the discontinuous change in the area A [for example, see Fig. 7(a) for $Pd^2/J_0 = 37.5$] at the transition temperature, and more interestingly, by a corre-
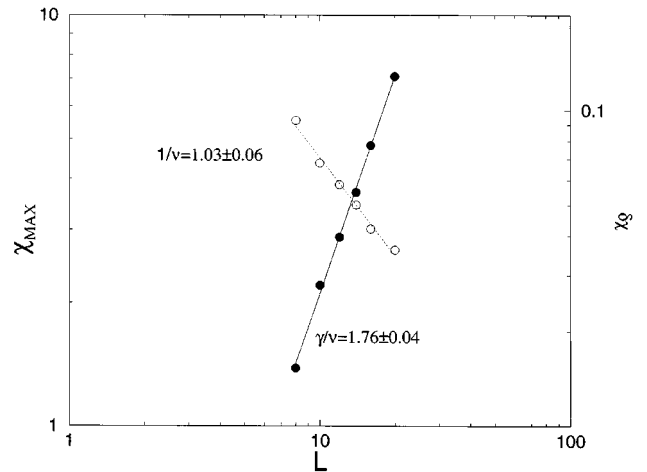

FIG. 10. Finite-size scaling plots for Ising model II for $Pd^2/J_0 = 20.0$. $\chi_{\max}$ is the maximum value of the spin susceptibility and $\delta\chi$ is the half width of the χ curve. The values of $\chi_{\max}$ and $\delta\chi$ were determined as described in the text. The value of the exponent γ/ν is 1.76 ± 0.04 and the value of the exponent $1/\nu$ is 1.03 ± 0.06.
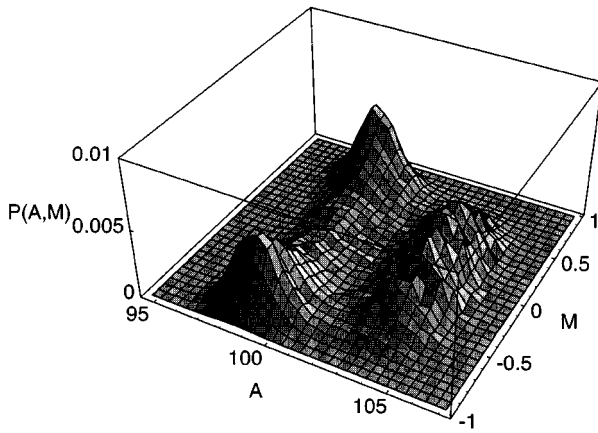
FIG. 11. Two-dimensional histogram $\mathcal{P}(A,M)$, where A is the total area of the system and M is the spin order parameter, obtained for Ising model II at parameter values $Pd^2/J_0=37.5$ and $T=1.012T_C$, where the spin singularity is coupled to the lattice melting. The system size is $N=256$. The histogram is obtained by extrapolation from a nearby temperature using the reweighting technique of Ferrenberg and Swendsen. The sampling time to obtain the histogram was 8 000 000 MCS.

sponding sharp change in the spin order parameter [see Fig. 8(a) for $Pd^2/J_0=37.5$] that is distinctly different from the temperature dependence of the spin order parameter at lower and higher values of the pressure. In order to demonstrate unambiguously that the spin order-disorder singularity is a *first-order* singularity, i.e., that it is slaved by the lattice melting, we have calculated the two-dimensional histogram $\mathcal{P}(A,M)$ (for a fixed system size), which is displayed in Fig. 11. The statistics underlying this histogram were obtained from 8×10^6 MCS [35]. The histogram clearly exhibits a two-state (spin-ordered and spin-disordered) structure, indicating coexisting SO and LD phases and a finite interfacial tension. Since the line of the critical spin transition is terminated from both the low-pressure and the high-pressure sides at t_1 and t_2, these two points are critical end points.

A last, but not the least important, observation we have made from the simulation data concerns the interplay between the two types of degrees of freedom in the low-pressure and the high-pressure regions. Although in these regions the first-order singularity associated with the translational degrees of freedom is decoupled from the critical singularity arising from the spin degrees of freedom, as manifested in the two separate transitions corresponding to the lattice melting and the critical spin transitions, respectively, there is evidence that the macroscopic behavior of one type of degrees of freedom is affected by the thermodynamic singularity arising from the other. For example, the critical spin fluctuations at the spin transitions, both in the low-pressure region and in the high-pressure region, enhance the density fluctuations, as indicated in Fig. 7(b) by the peaks in the area compressibility occurring at the spin transitions (although they are less pronounced than the peaks related to the lattice-melting transitions). Vice versa, at the lattice-melting transitions, the spin degrees of freedom are expected to display a weaker first-order singularity, the signature of which is too weak to be identified unambiguously from the simulation data.

A simple argument based on mainly mean-field considerations puts all the above observations and analysis into perspective, in relation to the phase behavior of Ising model I. As described in Sec. III, in Ising model II a new length scale R_0 is introduced to define the range of the spin-spin interaction. It is mainly the interplay between this new length scale and the length scale $l(P)$ set by the density (or pressure) of the system that gives rise to the phase behavior of Ising model II, which is more complex than that of Ising model I. If $l(P)$ is always smaller than R_0, then there is no difference between the thermal average values of the local coordination number and the number of the interacting nearest neighbors, whether the system is in a solid or liquid state; the phase behavior of Ising model II is effectively the same as the phase behavior of Ising model I. If, however, $l(P)$ for low pressures is larger than R_0, then the average value of the number of interacting nearest neighbors in the liquid state can be smaller than that in the solid state.

At very low pressures, the lattice melting takes place before any critical fluctuations in the spin degrees of freedom set in, taking the system from the SO phase to the LO phase. The critical spin transition occurs at a higher temperature, well separated from the lattice-melting transition, as in Ising model I. However, due to the reduced number of interacting particles in this case, the transition temperature is suppressed, compared to that of the solid-state critical spin transition. In this region of the phase diagram, the macroscopic behavior of the spin degrees of freedom is expected to have properties similar to the annealed and bond-diluted regular-lattice Ising model at low dilution [36]. As the pressure increases, the lattice-melting temperature increases and reaches at a point (t_1) the temperature of the critical spin transition, which is still lower than the critical temperature in the solid state. Beyond this point, the lattice-melting dictates the macroscopic behavior of the spin degrees of freedom, altering it discontinuously from the ordered state characteristic of the solid-state spin order parameter to the disordered state described by the bond-diluted and annealed (rather than the solid-state) Ising model and thereby rendering it a *first-order* singularity. At point t_2, the lattice-melting temperature coincides with the critical temperature of the solid-state (regular-lattice) Ising model and the first-order singularity in the spin degrees of freedom turns into the critical singularity again. In the high-pressure region, the lattice-melting temperature, being bounded from below by that of the noninteracting hard-disk system, is higher than the critical temperature for the magnetic transition. $l(P)$ becomes irrelevant to the critical magnetic transition, which separates the SO and SD phases. The phase behavior in this region is again similar to the phase behavior of Ising model I in the high-pressure region.

C. Model III: Doniach model on the random lattice

As discussed in the Introduction and Sec. III, model III, a Doniach model defined on the random lattice, was constructed as a minimal model that describes phase equilibria in phospholipid-bilayer systems that are characterized by translational degrees of freedom as well as internal degrees of freedom corresponding to the different conformational states of lipid-acyl chains. In this model, the spin degrees of freedom represent the chain conformational degrees of free-
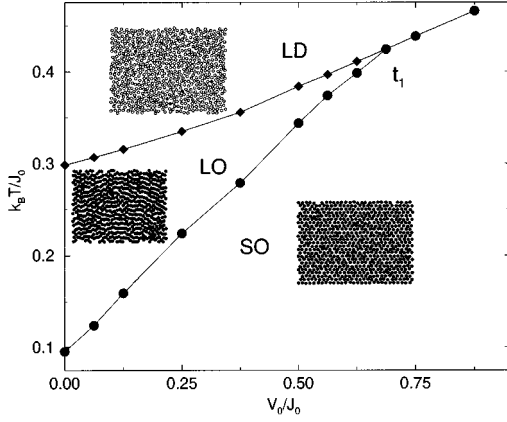
FIG. 12. Phase diagram for the extended Doniach model, model III. All three phase boundaries are first-order phase boundaries. The insets show snapshots of typical microconfigurations for the three different phases labeled SO (solid-ordered), LD (liquid-disordered), and LO (liquid-ordered). Chains in the disordered state are plotted as ○ and chains in the ordered chain state as ●. The three snapshots are not given to scale. In comparison with experiments the SO-LO phase line is interpreted as the submain phase transition and the LO-LD phase line as the main phase transition in long-chain phospholipid bilayers. t_1 is the triple point described in the text.

dom. The principal (dimensionless) parameters in the model are Pd^2/J_0, R_0/d, V_0/J_0, and $k_B T/J_0$ (see Fig. 3). Our simulation study of the model explored the two-dimensional parameter space spanned by V_0/J_0 and $k_B T/J_0$ for fixed values of the other two parameters $Pd^2/J_0 = 0.925$ and $R_0/d = 1.41$ and the simulation results are summarized in the phase diagram given in Fig. 12.

The topology of the phase diagram, characterized by three phase boundaries merging into a special point t_1, a triple point in this case, resembles the low-pressure part of the topology of the phase diagram of Ising model II, with the difference that the spin (or chain conformation) order-disorder transition in this model is first order, driven by the internal (or conformational) entropy and thus referred to as the chain-melting transition. This distinct topology indicates that, again, as in Ising model II, the thermodynamic singularity arising from the lattice melting can be either coupled or decoupled from the singularity associated with the chain melting, depending on the values of the parameters. The three phase boundaries, all being of first order and corresponding to a lattice-melting transition, a chain-melting transition, and a transition at which *both* melting processes take place, divide the explored region of the parameter space into three phases: the SO, LO, and LD phases. The three insets in the figure show, respectively, a characteristic microscopic configuration of each phase.

Figure 13 displays a selection of the simulation data that led to the construction of the above phase diagram. The data shown consist of the temperature dependence of the various thermodynamic quantities, the area per particle $\langle A \rangle$, the area compressibility K, the specific heat per particle C_P, and the enthalpy per particle $\langle H \rangle$ and were obtained for a system with $N = 256$ particles and for the following specific values of the model parameters: the internal entropy, $s = k_B \ln D_d = 14.4 k_B$; the conformational energy of the chain disordered state, $E_d/J_0 = 1.303$; and $V_0/J_0 = 0.25$. The data clearly in-
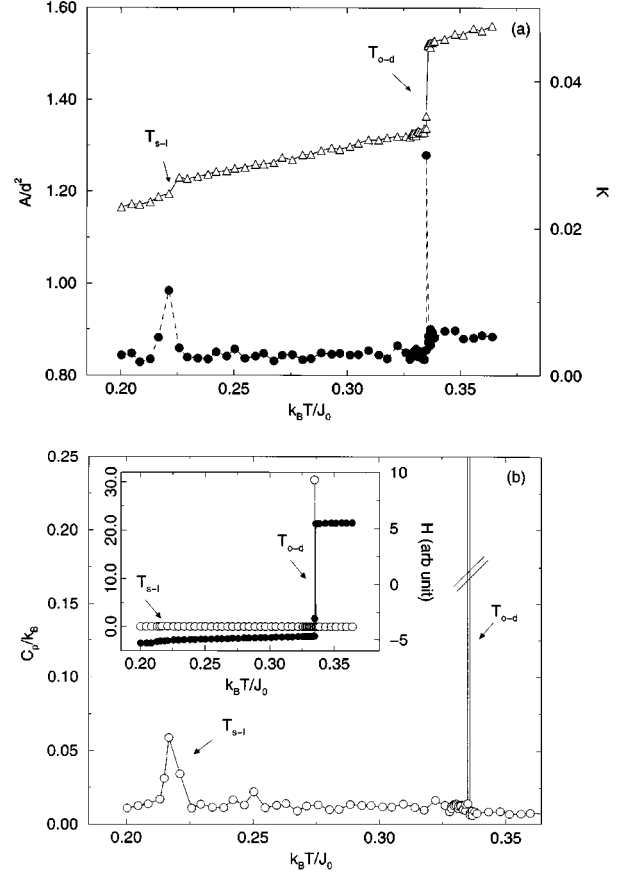

FIG. 13. Simulation data of the extended Doniach model, model III, for a system size of $N = 256$ and parameter values $Pd^2/J_0 = 0.925$, $V_0/J_0 = 0.25$, and $R_0/d = 1.41$. (a) shows the area per particle A (△) and the area compressibility K (●). (b) shows the heat capacity per particle C_P. The inset in (b) shows the full scale curves for the heat capacity (○) and the enthalpy per particle (- - -). $T_{o\text{-}d}$ is identified as the chain melting transition and $T_{s\text{-}l}$ as the submain transition in long-chain phospholipid bilayers.

dicate that two distinct first-order phase transitions take place at two different temperatures. At the lower temperature $T_{s\text{-}l} = 0.218 J_0/k_B$, a low-enthalpy, lattice-melting transition takes the system from the SO phase into the LO phase. At the higher temperature $T_{o\text{-}d} = 0.335 J_0/k_B$, the chain-melting transition changes the system from the LO phase to the LD phase.

Our calculation also showed that in the region of the parameter space where the two melting processes are decoupled, i.e., $V_0/J_0 < V_0/J_0|_{t_1}$, the temperature of the chain-melting transition $T_{o\text{-}d}$ actually depends on the model parameters in a rather simple way. Explicitly, $T_{o\text{-}d}$ can be determined as the solution to the equation

$$ -\frac{1}{2}\left[E_d + \frac{\langle z_i \rangle}{2}(J_0 + \langle q_i \rangle V_0) - k_B/T_{o\text{-}d}\ln D_d \right] + P\Delta\langle A \rangle = 0, \tag{21} $$

where $\langle z_i \rangle$ is the mean value of the local coordination number of the dynamic lattice and $\Delta\langle A \rangle$ is the change in the surface area per particle as the system undergoes the spin

order-disorder transition. $\langle q_i \rangle$ is the mean fraction of the nearest-neighbor pairs that interact with the strength of the deeper square well, a quantity that most significantly reflects the interplay between the translational and the chain-conformational degrees of freedom. It is rather straightforward to understand this result. The Hamiltonian of model III, as defined in Eq. (12), can be written as a (diluted) Ising model in an external temperature-dependent field, similar to the original Doniach lattice model, except that the field, which depends on z_i and q_i as

$$h_{(i)\text{eff}}(T) = -\frac{1}{2}\left[E_d + \frac{z_i}{2}(J_0 + q_i V_0) - k_B/T_{o\text{-}d}\ln D_d \right],$$

(22)

becomes a *fluctuating* quantity of the random lattice through the fluctuations in z_i and q_i. For the systems simulated with periodic boundary conditions, the local coordination number z_i is conserved on average, i.e., $\langle z_i \rangle = 6$. Furthermore, for a condensed 2D liquid system, z_i was found to have a very narrow distribution around 6. Similarly, the fluctuations of q_i about its mean value were also found to be small. Hence the chain-melting transition temperature is very well approximated by the temperature set by the condition $\langle h_{\text{eff}}(T_{o\,-d}) \rangle + P\Delta\langle A \rangle = 0$, which is simply that given by Eq. (21). For small values of V_0/J_0 the gap between the SO-LO and the LO-LD phase boundaries is quite large and the LO states close to the chain-melting transition contain many ''defects,'' interacting pairs having interparticle distances larger than R_0 and hence has a rather small value of $\langle q_i \rangle$. For instance, for $V_0/J_0 = 0.25$, we find $\langle q_i \rangle = 0.77$ for the LO states just below the chain-melting transition. As we move closer to t_1 the number of the defects in the LO states decreases and for $V_0/J_0 = 0.625$ we find $\langle q_i \rangle = 0.96$. Beyond the triple point $V_0/J_0|_{t_1}$ the low-temperature phase remains crystalline ordered, due to the strong interactions imposed by larger values of V_0, and the number of pair defects is essentially zero. An increase in temperature leads to the chain-melting process, which renders the particle-particle interaction ineffective and consequently brings about the lattice-melting process. Thus the phase boundary is essentially determined by the chain-melting process, for which Eq. (21), with $\langle q_i \rangle = 1$, still gives a largely valid description.

The enthalpy change across the lattice-melting transition can be found from the enthalpy histogram at the transition temperature. An estimate of the enthalpy change per particle $\Delta H_{s\text{-}l}$ leads to a value of approximately $0.35k_B$ per particle for the corresponding entropy change $\Delta S_{s\text{-}l}$. In contrast, the chain-melting transition exhibits a very large latent heat, corresponding to an entropy change per particle of approximately $14k_B$. The heat content in the lattice melting is thus only a few percent of the heat content in the spin order-disorder transition for the chosen set of model parameters.

The dependence of the lattice-melting transition temperature on V_0/J_0 is apparent in the phase diagram. The transitional entropy also was found to have a systematic dependence on the parameter. As the value of V_0/J_0 is increased from below towards the triple-point value, the simulation data given in Fig. 14 shows a steady increase in $\Delta S_{s\text{-}l}$ with the parameter value.
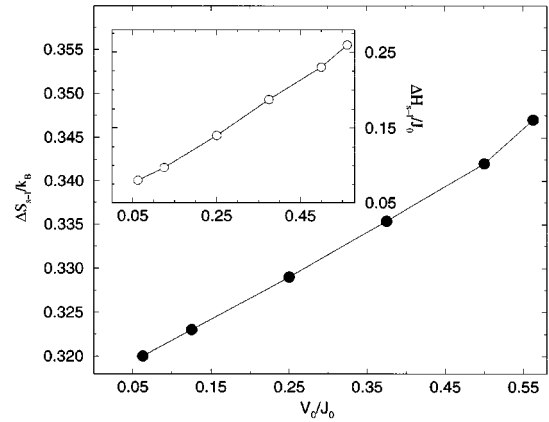

FIG. 14. Entropy change at the lattice-melting (or submain) transition $\Delta S_{s\text{-}l}$ for different values of the model parameter V_0/J_0 in model III (see Fig. 12). The inset gives the corresponding values of the transitional enthalpy $\Delta H_{s\text{-}l}$.

Our study of model III predicts for lipid-bilayer systems a rather generic picture of the phase behavior or, more specifically, of the mode in which the chain conformational and molecular translational degrees of freedom are coupled at macroscopic level. In particular, it is shown that the loss of the lateral (or in-plane) ordering, represented by the lattice-melting transition, can take place without the complete loss of the collective ordering in chain conformations; consequently, an intermediate phase, the LO phase, can exist [37]. There is no *a priori* reason why the lattice-melting transition and the chain-melting transition should synchronize, although it is generally accepted that the main transition in phospholipid bilayers involves both the lattice-melting and the chain-melting processes.

In a recent *high-sensitivity* calorimetric study by Jørgensen [40], a distinct submain transition was discovered to be present in fully hydrated multilamellar bilayers of long-chain lipids in the homologous series of di-acyl phosphatidylcholines DC$_n$PC, with $17 \leq n \leq 20$. The experimental data show that the entropy change per lipid molecule across this submain transition ΔS_{sm} is very small, being in the range between $0.22k_B$ and $0.56k_B$. Our model calculation offers an interpretation of this recently discovered submain transition as a decoupling of the lattice-melting transition from the chain-melting transition. As we have discussed in a recent paper [41], the latent heat or, correspondingly, the transitional entropy predicted by our study of model III for the lattice-melting transition compares favorably with the experimental data for the submain transition. This may imply that model III, despite its simplicity, has captured some of the essential mechanisms underlying the interplay between the chain conformational and the translational degrees of freedom in lipid-bilayer systems.

V. CONCLUSION

Motivated by the rich phase behavior of lipid-bilayer systems, the work reported in this paper has focused on investigating the equilibrium thermodynamic behavior in two-dimensional condensed many-particle systems where both translational and internal degrees of freedom are present and
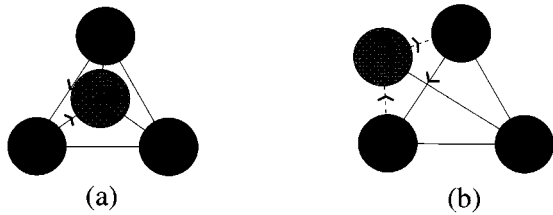
FIG. 15. Move from configuration (a) to configuration (b) that changes the orientation of the surface normal. The local orientation of the random lattice is indicated by the arrows on the tethers.

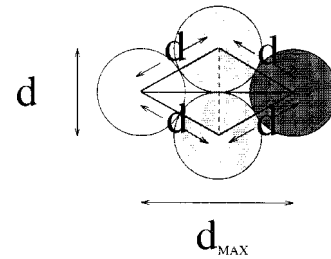FIG. 16. Extreme situation that may occur when $d_{max}/d > \sqrt{3}$. Hard disks are shown as circles and tethers between disks are shown as solid lines. When $d_{max}/d = \sqrt{3}$ two disks that are not connected by a tether can actually have a distance (shown by the dashed line) that is equal to d, the hard-disk diameter. When $d_{max}/d > \sqrt{3}$ the distance between nonconnected hard disks can be less than d.

are coupled through microscopic interactions. To this end, we first developed a random-lattice description of two-dimensional translational degrees of freedom. We then formulated, and studied using computer-simulation techniques, a series of three statistical-mechanical models, which describe the internal degrees of freedom essentially as the standard Ising model does the spin degrees of freedom, but have different emphasis and levels of complexity in the description of the coupling microscopic between the translational and internal (spin) degrees of freedom. These models were shown to lead to quite rich phase behavior, although they describe only microscopic interactions that are simple and generic. The most important feature in the phase behavior of these models is that, depending on the model parameters, thermodynamic singularities associated with the internal degrees of freedom can be either coupled to or decoupled from a first-order thermodynamic singularity in the collective behavior of the translational degrees of freedom that corresponds to a lattice-melting process, manifesting at the macroscopic level the interplay between the two types of degrees of freedom. In particular, as in Ising model II, when the internal degrees of freedom are strongly coupled to the translational degrees of freedom macroscopically, their order-disorder singularity is slaved by the first-order singularity of the lattice melting and becomes first order, in contrast to the critical singularity they exhibit when the coupling is weak at the macroscopic level. It is further shown that in the case of weak coupling, the universal critical behavior of the internal degrees of freedom remains unchanged and, in fact, is in the same universality class as the regular-lattice Ising model. Finally, we have discussed the prediction of one of the models, model III, in relation to a recent experimental observation of a (submain) phase transition in phospholipid-bilayer systems.

We conclude the paper with a final remark on the prospect of the type of random-lattice models as proposed in the paper. The formulations of such models are general and may be applied to any two-dimensional condensed systems where different types of degrees of freedom are present and relevant. In particular, this approach may open up new possibilities in studies of structural and thermodynamic properties of complex systems such as multicomponent lipid bilayers—a highly biologically relevant example being lipid-cholesterol mixtures [42]—and lipid-protein systems.

APPENDIX: TECHNICAL REMARKS ON THE ALGORITHM

This appendix contains a few remarks on the technical details of the implementation of the random-lattice algorithm described in Sec. II. The first remark concerns the question of how we establish a nearest-neighbor structure that is convenient for treatment of 2D systems of particles with short-range interactions. In off-lattice simulations, in contrast to lattice simulations, there exists no unique definition of nearest neighbors. The usual definition is the set of particles that lie within a certain distance of a given particle. The nearest-neighbor structure we have used differs from those constructed via other schemes of tessellation, e.g., Voronoi tessellation and Delauney and Dirichlet triangulation, of microscopic configurations of hard disks [43]. The local connectivity of our random lattice is constrained since the lattice is composed of hard disks of diameter d, connected by tethers that do not exceed a maximum length d_{max}. If d_{max} is within the range $d - \sqrt{3}d$, the link structure of the network provides an easy access to local distribution of particles and a good representation of a nearest-neighbor structure. Since d_{max} is rescaled during the simulation, d_{max}/d can sometimes exceed $\sqrt{3}$ as the simulation proceeds. However, with an appropriately chosen range of values for the lateral pressure P, those configurations will have negligible effect on the thermodynamic properties of the system.

The second remark relates to a situation that could, in principle, arise, where the link structure cannot be directly used to represent the local particle distribution. To illustrate the situation, we define an inside-outside orientation of a triangular surface element by associating with it a normal vector. If $d_{max}/d \leq \sqrt{3}$, the sense of local orientation of any triangular element of the network stays the same throughout a simulation. Thus an inside-outside orientation across the whole surface is well defined. If, however, $d_{max}/d > \sqrt{3}$, a random move that changes the local orientation of a triangular element, leading to local overlapping of triangles, then becomes possible, as depicted in Fig. 15. Such moves are

excluded in the simulation algorithm; only those moves that preserve the inside-outside orientation of the surface are accepted.

The last remark deals with the practical implementation of the hard-disk condition for the particles. A rigorous implementation of the condition would, in principle, require building up a cell structure that encompasses the whole system [26]. However, such a procedure would require a considerable amount of computing time and would significantly reduce the efficiency of the algorithm. We have therefore employed a faster, although not as rigorous, method by which we only check those particles that are directly linked by one tether and those that are connected by two successive tethers.

If $d_{max}/d > \sqrt{3}$ it is obviously not sufficient only to check whether the hard-disk condition is violated by particles that are linked by tethers, since the random moves of particles can lead to situations where two particles are physically closer than the distance of the hard-disk diameter d without being connected by a tether (see Fig. 16). By extending the check for violation of the hard-disk condition to particles connected by two successive tethers we can, provided that d_{max}/d is not too much larger than $\sqrt{3}$, ensure that no two particles violate the hard-disk condition. As an example, we have found that for $d_{max}/d = 1.85$ only approximately 1 in 10 000 microconfigurations violates the hard-disk condition.

[1] J. Prost and P.-G. de Gennes, *Liquid Crystals* (Clarendon, Oxford, 1993).

[2] M. Bloom, E. Evans, and O.G. Mouritsen, Q. Rev. Biophys. **24**, 293 (1991).

[3] O.G. Mouritsen, Chem. Phys. Lipids **57**, 179 (1991).

[4] S. Doniach, J. Chem. Phys. **68**, 4912 (1978).

[5] O.G. Mouritsen, B. Dammann, H.C. Fogedby, J.H. Ipsen, C. Jeppesen, K. Jørgensen, J. Risbo, M.C. Sabra, M.M. Sperotto, and M.J. Zuckermann, Biophys. Chem. **55**, 55 (1995).

[6] M. Vist and J.H. Davis, Biochemistry **29**, 451 (1990).

[7] J.H. Ipsen, G. Karlström, O.G. Mouritsen, H. Wennerström, and M.J. Zuckermann, Biochem. Biophys. Acta **905**, 162 (1987).

[8] J.H. Ipsen, O.G. Mouritsen, and M.J. Zuckermann, Biophys. J. **56**, 661 (1989).

[9] Recent molecular-dynamics calculations for pure lipid bilayers in both the SO and LD include H. Heller, K. Scheaffer, and K. Schulten, J. Phys. Chem. **97**, 8343 (1993); S.-W. Chu, M. Clark, V. Balaj, S. Subramanian, H.L. Scott, and E. Jakobsson, Biophys. J. **69**, 1230 (1995); K. Tu, D.J. Tobias, and M.L. Klein, *ibid.* **69**, 2258 (1995); K. Tu, D.J. Tobias, J.K. Blasie, and M.L. Klein, *ibid.* **70**, 565 (1996). However, such studies cannot as yet be used to examine the regions of the phase transition due to the unrealistically large calculational time required.

[10] An Euler characteristic of the regular triangular lattice with periodic boundary conditions is $\chi = N - L_E + N_T = 0$, where N is the number of lattice sites, L_E is the number of bonds, and N_T is the number of triangles.

[11] D.V. Boulatov and V.A Kazakov, Phys. Lett. B **186**, 379 (1987).

[12] R. Ben-av, J. Kinar, and S. Solomon, Int. J. Mod. Phys. **3**, 279 (1992).

[13] M. Vekić, S. Liu, and H.W. Hamber, Phys. Lett. B **329**, 444 (1994).

[14] D. Boal and M. Rao, Phys. Rev. A **45**, 6947 (1992).

[15] D.M. Kroll and G. Gompper, Phys. Rev. A **46**, 3119 (1992).

[16] C. Jeppesen and J.H. Ipsen, Europhys. Lett. **22**, 713 (1993).

[17] D. Boal, U. Seifert, and A. Zilker, Phys. Rev. Lett. **69**, 3405 (1992).

[18] B. Dammann, H.C. Fogedby, J.H. Ipsen, O.G. Mouritsen, J. Risbo, M.C. Sabra, M. Sperotto, and M.J. Zuckermann, in *Nonmedical Applications of Liposomes*, edited by Y. Barenholz and D. Lasic (CRC, Boca Raton, FL, 1995), p. 85.

[19] O.G. Mouritsen, in *Molecular Description of Biological Membrane Components by Computer Aided Conformational Analysis*, edited by R. Brasseur (CRC, Boca Raton, FL, 1990), Vol. 1, p. 3.

[20] In the simulations we found that the variations in the value of $\langle d_{max}/d \rangle$ were very small. For the systems with the largest change in density the value of $\langle d_{max}/d \rangle$ was 1.80 for the lowest density in the simulation and 1.59 for the highest density. Thus, even in the high-density regime the system is far from the completely constrained limit $\langle d_{max}/d \rangle = 1.0$.

[21] A.M. Ferrenberg and R.H. Swendsen, Phys. Rev. Lett. **61**, 2635 (1988).

[22] A.M. Ferrenberg and R.H. Swendsen, Phys. Rev. Lett. **63**, 1195 (1989).

[23] C. Jeppesen (private communication).

[24] J. Lee and K.J. Strandburg, Phys. Rev. B **46**, 11 190 (1992).

[25] J.F. Fernández, J.J. Alonso, and J. Stankiewicz, Phys. Rev. Lett. **75**, 3477 (1995).

[26] M.P. Allen and J.P. Tildesley, *Computer Simulations of Liquids* (Oxford University Press, New York, 1987).

[27] K.J. Strandburg, Rev. Mod. Phys. **60**, 161 (1988); **61**, 747(E) (1989).

[28] Béla Joós, in *Dislocations in Solids*, edited by F.R.N. Nabarro and M.S. Duesbery (North-Holland, Amsterdam, in press), Vol. 10.

[29] D.R. Nelson and B.I. Halperin, Phys. Rev. B **19**, 2457 (1979); A.P. Young, *ibid.* **19**, 1855 (1979).

[30] J.M. Kosterlitz and D.J. Thouless, J. Phys. C **6**, 1181 (1973); V.L. Berenzinskii, Zh. Éksp. Teor. Fiz. **59**, 907 (1970); **61**, 1144 (1971) [Sov. Phys. JETP **32**, 493 (1971); **34**, 610 (1972)].

[31] A.E. Ferdinand and M.E. Fisher, Phys. Rev. **185**, 832 (1969).

[32] More accurate values of these three quantities can obviously be obtained by performing longer simulations in conjunction with the Ferrenberg-Swendsen reweighting technique [21]. For the present purpose, it is sufficient to use the peak position and the height of the response functions as estimates for $\chi_{max}(L)$, $C_{P,max}(L)$, and $\delta\chi(L)$.

[33] H.E. Stanley, *Introduction to Phase Transitions and Critical Phenomena* (Clarendon, Oxford, 1971).

[34] To determine the precise locations of the two critical end points requires a detailed analysis based on finite-size scaling theory, which, however, is computationally very demanding

and beyond the scope of the present work. The important point is that we were able to establish the existence of these two points.

[35] A more satisfactory analysis would be a detailed finite-size scaling analysis of the two-dimensional histogram $\mathcal{P}(A,M)$. However, due to the extensive statistics that an analysis of this kind would require, we have not performed such a systematic finite-size scaling analysis.

[36] R.B. Stinchcombe, in *Phase Transitions and Critical Phenomena*, edited by C. Domb and J.L. Lebowitz (Academic, New York, 1983), Vol. 7.

[37] The phase diagram for model III (the Doniach model) of Fig. 12, which is applicable to the phase behavior of pure lipid bilayers, is given in terms of the SO, LO, and LD phases. The generic phase behavior shown in this diagram was first found using a lattice model [38] that combined a Pink model [39] and a 30-state Potts model. The pink model is an extension of the Doniach model involving ten conformational states and thus describes the chain degrees of freedom, while the Potts model represents the translational degrees of freedom. The combined Pink-Potts model was examined on a regular lattice and therefore cannot give a true physical representation of the lattice melting.

[38] O.G. Mouritsen and M.J. Zuckermann, Eur. Biophys. J. **15**, 77 (1987).

[39] D.A. Pink, T.J. Green, and D. Chapman, Biochemistry **19**, 349 (1980).

[40] K. Jørgensen, Biochim. Biophys. Acta **1240**, 111 (1995).

[41] M. Nielsen, L. Miao, J.H. Ipsen, K. Jørgensen, M.J. Zuckermann, and O.G. Mouritsen, Biochem. Biophys. Acta **1283**, 170 (1996).

[42] M. Nielsen, L. Miao, J.H. Ipsen, M.J. Zuckermann, and O.G. Mouritsen (unpublished).

[43] D.P. Fraser, M.J. Zuckermann, and O.G. Mouritsen, Phys. Rev. A **42**, 3186 (1990).